10. E. Martinez, T. K. Kundu, J. Fu, R. G. Roeder, *J. Biol. Chem.* **273**, 23781 (1998).
11. P. A. Grant *et al.*, *Cell* **94**, 45 (1998).
12. For immunoprecipitation, mouse monoclonal antibodies (mAbs), anti-hTAF$_{II}$30 1H8 (*8*), and anti-hTBP 2C1 (*5*), were purified as described in (*4*). HeLa cell nuclear extract was first passed through a single-stranded (ss) DNA cellulose column to eliminate proteins that bind nonspecifically to the resin used later in immunoprecipitations. Fractions were immunoprecipitated with mAbs bound to protein G–Sepharose (Pharmacia) as described in (*8*). These complexes bound to protein G–Sepharose were washed three times with IP buffer [25 mM tris-HCl (pH 7.9), 10% (v/v) glycerol, 0.1% NP-40, 0.5 mM dithiothreitol, 5 mM $MgCl_2$] containing 500 mM KCl and two times with IP buffer containing 100 mM KCl. After washing, bound proteins were eluted with a 1000-fold excess of the corresponding epitope peptide and analyzed by SDS–polyacrylamide gel electrophoresis (SDS-PAGE). The polypeptide composition of the isolated complexes were verified either on silver-stained SDS-PAGE gels or by protein immunoblots as described (*1*, *8*).
13. The following subunits were identified in hTFIID: TBP, TAF$_{II}$250, TAF$_{II}$150, TAF$_{II}$135, TAF$_{II}$100, TAF$_{II}$80, TAF$_{II}$55, TAF$_{II}$31, TAF$_{II}$30, TAF$_{II}$28, TAF$_{II}$20, and TAF$_{II}$18. The hTFTC complex contained TAF$_{II}$150, TAF$_{II}$135, TAF$_{II}$100, TAF$_{II}$80, TAF$_{II}$55, TAF$_{II}$31, TAF$_{II}$30, TAF$_{II}$20, TAF$_{II}$18, GCN5-L, PAF65β (*9*), hADA3, hSPT3, TRRAP, and other noncharacterized subunits (*1*).
14. We cross-linked 5 μl of the purified TFTC or TFIIDβ preparations for 10 s with 0.05% glutaraldehyde and placed them on a 10-nm-thick carbon film previously treated by a glow discharge in air. After 2 min of adsorption, the grid was negatively stained with a 2% uranyl acetate solution. The images were formed on a Philips CM120 Transmission Electron Microscope operating at 100 kV and were analyzed as described (*16*).
15. M. van Heel, G. Harauz, E. V. Orlova, *J. Struct. Biol.* **116**, 17 (1996).
16. C. Klinger *et al.*, *EMBO J.* **15**, 4643 (1996).
17. M. van Heel and J. Frank, *Ultramicroscopy* **6**, 187 (1981).
18. A. K. P. Taggart and B. F. Pugh, *Science* **272**, 1331 (1996).
19. A. Hoffmann *et al.*, *Nature* **380**, 356 (1996).
20. X. Xie *et al.*, *Nature* **380**, 316 (1996).
21. Y.-G. Gangloff *et al.*, *Mol. Cell. Biol.*, in press.
22. C. Birck *et al.*, *Cell* **94**, 239 (1998).
23. T. Oelgeschlager, C. M. Chiang, R. G. Roeder, *Nature* **382**, 735 (1996).
24. A. Hoffmann, T. Oelgeschlager, R. G. Roeder, *Proc. Natl. Acad. Sci. U.S.A.* **94**, 8928 (1997).
25. M. Radermacher, T. Wagenknecht, A. Verschoor, J. Frank, *J. Microsc.* **146**, 113 (1987).
26. The 3D models were calculated from conical tilt series produced by recording the same field of molecules at 60° and 0° tilt. Molecular images were extracted from the untilted micrographs, aligned, and classified into homogeneous groups to identify subpopulations of similarly oriented particles. Tilt and in-plane rotation parameters yield the Euler angles for each tilted view, about 100 of which were merged by filtered back-projection to calculate the 3D molecular envelope.
27. S. A. Darst, A. M. Edwards, E. W. Kubalek, R. D. Kornberg, *Cell* **66**, 121 (1991).
28. B. A. Purnell, P. A. Emanuel, D. S. Gilmour, *Genes Dev.* **8**, 830 (1994).
29. R. E. Kingston, *Nature* **399**, 199 (1999); M. Hampsey and D. Reinberg, *Curr. Opin. Genet. Dev.* **9**, 132 (1999).
30. Y. Nakatani, S. Bagby, M. Ikura, *J. Biol. Chem.* **271**, 6575 (1996).
31. D. Liu *et al.*, *Cell* **94**, 573 (1998).
32. P. Schultz, H. Celia, M. Riva, A. Sentenac, P. Oudet, *EMBO J.* **12**, 2601 (1993).
33. T. K. Kim *et al.*, *Proc. Natl. Acad. Sci. U.S.A.* **94**, 12268 (1997).
34. M. van Heel, *Ultramicroscopy* **21**, 95 (1987).
35. We thank Y. Lutz for antibody production, J. C. Dantonel and B. Bell for discussions and critical reading of the manuscript, P. Eberling for peptide synthesis, the cell culture group for HeLa cells, J. C. Homo for help with electron microscopes, and R. Buchert, J.-M. Lafontaine, and B. Boulay for illustrations. M.B. was supported by a fellowship from the Ministère de la Recherche et Technologie. This work was supported by grants from CNRS, INSERM, the Hôpital Universitaire de Strasbourg, Fondation pour la Recherche Médicale, the Association pour la Recherche contre le Cancer, the Ligue National Contre le Cancer, and the Human Frontier Science Program.

11 August 1999; accepted 10 November 1999

Three-Dimensional Structure of the Human TFIID-IIA-IIB Complex

Frank Andel III,[1] Andreas G. Ladurner,[3] Carla Inouye,[3] Robert Tjian,[2] Eva Nogales[1,3]*

The multisubunit transcription factor IID (TFIID) is an essential component of the eukaryotic RNA polymerase II machinery that works in concert with TFIIA (IIA) and TFIIB (IIB) to assemble initiation complexes at core eukaryotic promoters. Here the structures of human TFIID and the TFIID-IIA-IIB complex that were obtained by electron microscopy and image analysis to 35 angstrom resolution are presented. TFIID is a trilobed, horseshoe-shaped structure, with TFIIA and TFIIB bound on opposite lobes and flanking a central cavity. Antibody studies locate the TATA-binding protein (TBP) between TFIIA and TFIIB at the top of the cavity that most likely encompasses the TATA DNA binding region of the supramolecular complex.

The accurate and regulated transcription of protein coding genes in all eukaryotic organisms requires the assembly at specific promoter elements of a complex molecular machine that includes general transcription factors in association with RNA polymerase II (RNA pol II) (*1*). Recognition of core promoter DNA sequences by TFIID (*2*) is followed by the assembly of a fully activated preinitiation complex that contains TFIIA, TFIIB, TFIIE, TFIIF, TFIIH, and RNA pol II (*3*). In the absence of activators bound to enhancer elements, this core transcription complex can accurately initiate basal levels of RNA synthesis. In the presence of gene-selective enhancer and promoter binding activators, significantly elevated levels of transcription initiation can be achieved. A key step in the multistep process of gene activation is the recruitment and assembly of the TFIID-IIA-IIB complex at the TATA DNA region that is found in many core promoters of eukaryotic genes. The TBP subunit and some of the TBP-associated factors (TAF$_{II}$) subunits (TAF$_{II}$250, TAF$_{II}$150, and TAF$_{II}$70) make specific contacts with the TATA box and other core promoter elements, including initiator (INR) and downstream promoter elements (DPE) (*4*). Other TAF$_{II}$'s of the multisubunit TFIID complex such as TAF$_{II}$130, -100, -55, -32, -30, and -28 likely serve as targets of activation domains involved in the recruitment and stabilization of TFIID at core promoters by upstream enhancer binding factors (*5*–*7*).

The binding of TFIID to the core promoter is coordinated with the assembly of an active preinitiation complex that includes IIA and IIB. X-ray diffraction and nuclear magnetic resonance (NMR) studies have revealed the structures of various subdomains and truncated fragments of IIA and IIB and of subunits contained within TFIID. For example, the high-resolution structures of TBP bound to TATA DNA and to domains of either IIA or IIB have been determined (*8*). However, both the size of the complex and the inherent difficulties in obtaining large quantities of purified holo-TFIID, -IIA, and -IIB have precluded conventional x-ray diffraction studies of the full complex. Consequently, the overall shape and relative position of the components within the TFIID-IIA-IIB complex remain unknown. As a first step toward determining the structure of the intact native human TFIID, we used electron microscopy (EM) and single-particle image analysis to obtain the structure of TFIID and its complex with full-length IIA and IIB at 35 Å resolution.

Homogeneous preparations of TFIID suitable for EM studies were purified as described (*9*). For preparations of TFIID bound to IIB and IIA, recombinant IIB and IIA subunits were purified and reconstituted with antibody affinity-purified TFIID in vitro (*10*–

[1]Life Science Division, Lawrence Berkeley National Laboratory, Berkeley, CA 94720, USA. [2]Howard Hughes Medical Institute, [3]Molecular and Cell Biology Department, University of California, Berkeley, CA 94720, USA.

*To whom correspondence should be addressed. E-mail: enogales@lbl.gov

12). The activity of purified TFIID, IIA, and IIB was confirmed by in vitro transcription assays (Fig. 1A). Preparations of holo-TFIID containing the full complement of TAFs were highly active in mediating Sp1-dependent transcription (Fig. 1B) when reconstituted with all the necessary general factors and the coactivator CRSP (*11, 13*). These functionally active preparations of TFIID, IIA, and IIB were used for EM analysis.

Electron microscopy grids of TFIID (~45 ng/μl) were prepared and stained with uranyl acetate (4%). To obtain an initial three-dimensional (3D) reconstruction, we collected image pairs of tilted (32°) and untilted (0°) samples with the use of the random conical tilt method (*14*). Images were obtained under low-dose conditions, with the use of a JEOL 4000EX electron microscope at ×30,000 magnification with a defocus of 1 μm. Micrographs showed that the native human TFIID preparation was homogenous (Fig. 2A). Each micrograph contained ~300 particles. The micrographs were digitized with a scan step of 21 μm (corresponding to a pixel size in the sample of 7 Å). Image analysis was carried out with the WEB and SPIDER software packages (*15*). A total of 4418 particle image pairs were windowed (64 pixels by 64 pixels) and were used for further processing. Untilted images were subjected to reference-free alignment and merged by performing in-plane shifts and rotations into 25 classes defined by K-means clustering (*16*). The large number of classes chosen reflects the fact that TFIID orients almost randomly on the carbon film. 3D structures for each of the 25 classes were calculated by back projection using the paired tilted images. Twenty-four of the classes showed excellent correlation ($R > 0.85$), thus a single 3D structure was obtained with the single particle–tilted images from these 24 classes. This initial structure served as a reference for angular refinement (*17*). Eighty-three reference projections were computed from the crude volume, with a difference in view angle of 15°. The untilted particle images were matched to the reference projections on the basis of highest cross-correlation by performing in-plane rotations and shifts. A refined volume was then calculated with the newly identified Euler angles. This procedure was repeated twice. Final angular refinement was performed by generating 5088 reference projections from the newly obtained structure with an angular step of 2°. The projection images of TFIID cover the full range of angular distribution (Fig. 2B). The final refined structure is depicted from six viewing angles (Fig. 3). The structure has been rendered to correspond to the molecular mass estimated for TFIID (775 kD). The reconstruction has a resolution of 35 Å, based on the 0.5 Fourier shell correlation criteria (*18*).

The 3D reconstruction of TFIID reveals a horseshoe-shaped structure (roughly 200 Å by 135 Å by 110 Å) consisting of three main lobes, A, B, and C. These lobes are connected by narrower bridges (~20 Å wide) and arranged around a cavity 65 Å in diameter (Fig. 3). The lobes are roughly equal in size (~60 Å in diameter) but differ in structural detail. Above the connecting bridges and between the lobes are two V-shaped channels, one ~25 Å across (large arrow in Fig. 3, D and E) and the other ~15 Å across (small arrow in Fig. 3, D and F), that separate the lobes on the front face. The central cavity and its 40 Å open channel at the bottom of the horseshoe could easily accommodate a strand of double-helical DNA 20 Å in diameter.

The 3D structure of the binary complex, TFIID-IIB, was obtained by mixing the two factors in equimolar concentrations and incubating them for 1 hour at 4°C. Sample preparation, data collection, and image analysis were as described for holo-TFIID. As for TFIID alone, the dimeric TFIID-IIB complexes were randomly oriented on the carbon support of the EM grid. Four thousand individual particle images were aligned three-dimensionally by reference to the refined 35 Å structure of naked TFIID (the molecular weight of IIB is 4% that of holo-TFIID). Once Euler angles were assigned, the new particle images were back-projected to generate a reconstruction of the TFIID-IIB complex that was used as reference for further angular refinement to a resolution of ~35 Å. The structures of TFIID and the TFIID-IIB complex were then normalized according to the TFIID protein density, scaled, and subtracted to generate a difference map corresponding to the density of IIB (green in Fig. 4A). Part of the density attributable to IIB lies within the TFIID density. This may reflect a structural change in TFIID upon binding of

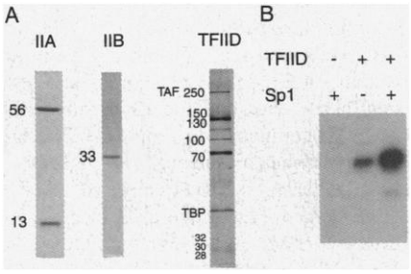

Fig. 1. (**A**) Silver-stained SDS–polyacrylamide gel electrophoresis gels of recombinant IIA, IIB, and immunopurified native TFIID. The apparent molecular weight of each polypeptide is indicated to the left of each panel. (**B**) Reconstituted transcription reactions with the $(GC)_3$-BCAT template, supplemented with TFIID or Sp1, or both, as indicated. The final products were analyzed by primer extension.

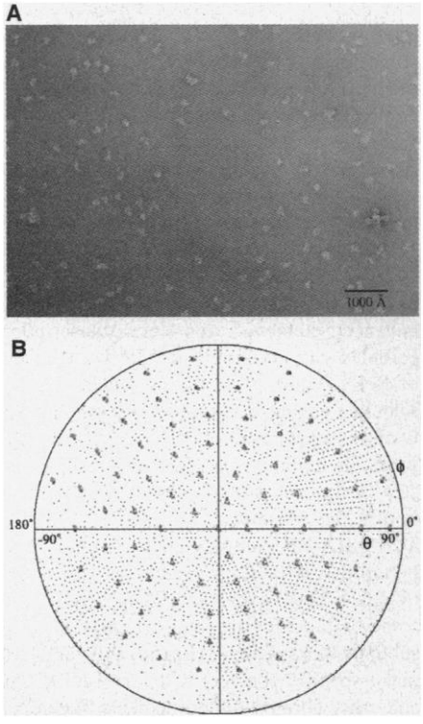

Fig. 2. (**A**) Electron micrograph of negatively stained human TFIID. TFIID particles appear in a variety of orientations on the carbon support. (**B**) Angular distribution of the different projections (views) of TFIID used to generate the 3D structure shown in Fig. 3. Some of the different views are shown for reference. The diagram shows that the reconstruction of TFIID is free of missing cone artifacts. The same applies to the reconstructions obtained from TFIID-IIB and TFIID-IIA-IIB complexes (*25*).

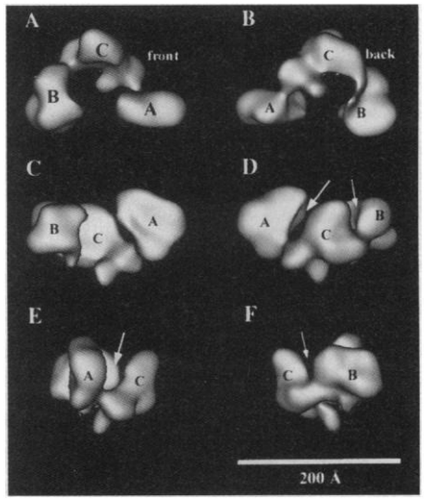

Fig. 3. 3D reconstruction of human TFIID at 35 Å resolution. (**A**) and (**B**) are front and back views, respectively, showing the overall horseshoe structure of TFIID. The three lobes have been designated A, B, and C. (**C**) through (**F**) are side views obtained by turning the front view in (A) out of the paper by 90°, then rotating around a horizontal axis through the center of the cavity. The V-shaped channels between lobes are indicated by arrows.

IIB, or a differential staining in the two samples. The difference density is positioned mainly on lobe B, close to the ~15 Å bridge connecting it with lobe C.

The 3D structure of the ternary complex TFIID-IIA-IIB was obtained with the use of the same procedure as for the TFIID-IIB complex. Equimolar concentrations of the three components were incubated. A total of 5000 particle images were used to obtain a reconstruction at ~35 Å resolution. The difference map obtained between TFIID and TFIID-IIA-IIB (Fig. 4B) contains two distinct regions of density: one corresponding to the location of the difference obtained in the presence of IIB alone (green) and a second one in lobe A consisting of a cluster of differentiated densities (magenta). This result confirms the position of IIB and identifies the location of IIA. Three main densities in the difference map can be attributed either to the binding of IIA or to conformational changes in TFIID upon binding of IIA. One of these densities constitutes a new bridge between lobes A and C, which occupies part of the central cavity. If this cavity is involved in binding the core promoter, then this bridge of density might affect the stability of the TFIID-DNA complex, in agreement with the enhanced DNA binding of TFIID by IIA (*19*). The subunits of IIA bind to TFIID on the opposite side of the central cavity relative to the IIB binding site, similar to the binding of IIB and IIA to the opposite "stirrups" of TBP (*8*). The location of IIA and IIB on different regions of the TFIID structure suggests that these factors could influence the overall shape of the preinitiation complex and, in particular, the shape of the putative DNA binding cavity, from two different ends of the complex.

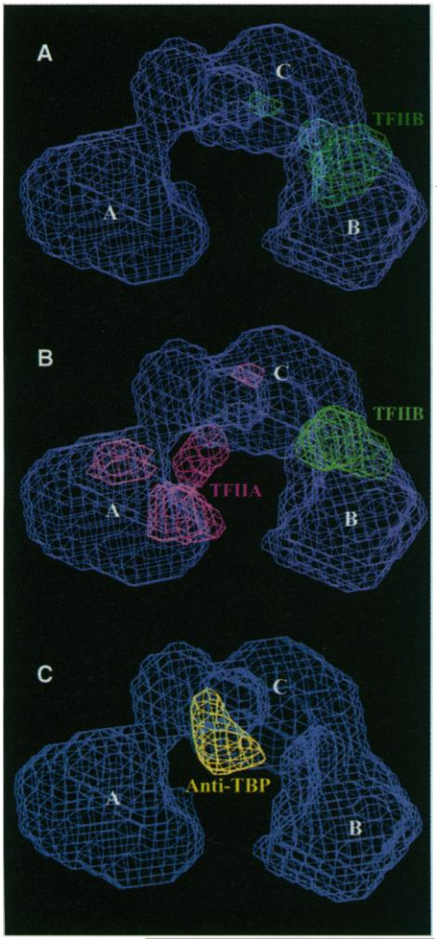

Fig. 4. Position of IIB and IIA on the TFIID structure and mapping of the TBP. The blue mesh corresponds to the holo-TFIID, with the A, B, and C lobes indicated. (**A**) The green mesh corresponds to the density difference between the holo-TFIID and the TFIID-IIB complex. (**B**) The magenta and green meshes show the density difference between the holo-TFIID and the trimeric complex TFIID-IIA-IIB. The density depicted in light green can be attributed to TFIIB by comparison with (A), and the magenta density therefore corresponds to IIA. (**C**) The yellow mesh shows the density difference between the holo-TFIID and TFIID that is bound to the TBP antibody.

The crystal structure of TBP bound to IIA and IIB suggested that TBP should bind in the central domain C, between these two general factors (*8*). To test this hypothesis, we employed a monoclonal antibody raised against TBP (anti-TBP) (*20*). TFIID–anti-TBP binding and preparation for EM were performed as described for the TFIID-IIB complex, using a 5:1 anti-TBP:TFIID ratio. More than 9000 particle images of the TFIID-anti-TBP complex were used to obtain a reconstruction at ~30 Å resolution. Figure 4C indicates the position of the bound anti-TBP obtained in the difference map applying the same methodology we used to find the IIA and IIB binding positions. The binding site of anti-TBP indicates that TBP resides at the top of the cavity within the central domain C and faces the cavity in a position between IIA and IIB. We propose that TFIID binds the core promoter within the central cavity at the central lobe C through TBP.

The structure of the TFIID-IIA-IIB complex, together with the existing knowledge of the interaction between different TAFs and other components of the initiation complex, suggest a hypothetical distribution of TAFs on the three lobes of the TFIID structure. Lobe A is likely to contain TAF130, which is known to interact with IIA (*21*), whereas TAF32 might form part of lobe B because of its interaction with IIB (*22*). Because IIB is known to contact RNA pol II (*23*), we suspect that lobe B may be a major interaction region for polymerase. TAF250, which interacts with TBP and contributes multiple contacts for the assembly of the complex (*7, 24*), is expected to form a major part of lobe C. Finally, TAF18, -20, and -28 may also be located in lobe C, because they have been reported to interact directly with TBP (*7*).

The EM studies presented here reveal a model for the structure of TFIID complexed to both IIA and IIB in the absence of DNA. Our findings provide a 35 Å structure of TFIID and the binding locations of IIA and IIB in relation to the larger TFIID. Antibody mapping of TBP within TFIID strongly suggests that the binding position of DNA is at the top of the central cavity within the TFIID complex. The horseshoe shape of TFIID and its trilobal structure suggest conformational flexibility around the narrow contact regions. The orientation between the lobes is probably regulated by transcriptional factors, and this would affect the shape of the central cavity and the binding to DNA. IIA and IIB reside on opposite sides of TFIID and are likely to stiffen the structure of TFIID by bridging different lobes. IIA binds across the 25 Å channel near the surface of the central cavity. Thus, IIA could increase the surface available for DNA binding and affect the affinity of TFIID-IIA for DNA that has been observed in DNA binding studies.

References and Notes

1. R. Tjian and T. Maniatis, *Cell* **77**, 5 (1994); R. G. Roeder, *Trends Biochem. Sci.* **21**, 327 (1996); D. Reinberg *et al.*, *Cold Spring Harbor Symp. Quant. Biol.* **63**, 83 (1998); M. Hampsey and D. Reinberg, *Curr. Opin. Genet. Dev.* **9**, 132 (1999).
2. S. Hahn *et al.*, *Cell* **58**, 1173 (1989); M. Horikoshi *et al.*, *Nature* **341**, 299 (1989); M. G. Peterson *et al.*, *Science* **248**, 1625 (1990).
3. S. Buratowski *et al.*, *Cell* **56**, 549 (1989).
4. N. Nakajima, M. Horikoshi, R. G. Roeder, *Mol. Cell. Biol.* **8**, 4028 (1988); B. D. Dynlacht, T. Hoey, R. Tjian, *Cell* **66**, 563 (1991); J. L. Chen *et al.*, *Cell* **79**, 93 (1994); J. A. Goodrich, G. Cutler, R. Tjian, *Cell* **84**, 825 (1996); C. P. Verrijzer and R. Tjian, *Trends Biochem. Sci.* **21**, 338 (1996); Y. Tao *et al.*, *J. Biol. Chem.* **272**, 6714 (1997); W. C. Shen and M. R. Green, *Cell* **90**, 615 (1997); T. W. Burke and J. T. Kadonaga, *Genes Dev.* **11**, 3020 (1997); J. Kaufmann *et al.*, *Mol. Cell. Biol.* **18**, 233 (1998).
5. J. L. Chen *et al.*, *Cell* **79**, 93 (1994).
6. J. A. Goodrich and R. Tjian, *Curr. Opin. Cell Biol.* **6**, 403 (1994); J. Adnane, Z. Shao, P. D. Robbins, *Oncogene* **18**, 239 (1999); A. C. Lavigne *et al.*, *Mol. Cell. Biol.* **19**, 5486 (1999).
7. G. Mengus *et al.*, *EMBO J.* **14**, 1520 (1995).
8. D. B. Nikolov *et al.*, *Nature* **377**, 119 (1995); S. Tan *et al.*, *Nature* **381**, 127 (1996); J. H. Geiger *et al.*, *Science* **272**, 830 (1996).
9. We subjected 200 liters of HeLa cell nuclear extracts to phosphocellulose chromatography, followed by antibody affinity purification using a monoclonal antibody directed against the $TAF_{II}130$ subunit of human TFIID (anti-$TAF_{II}130$). The highly purified TFIID was eluted from the affinity resin with an epitope peptide specifically recognized by anti-$TAF_{II}130$ (*10*).
10. A. M. Näär *et al.*, *Genes Dev.* **12**, 3020 (1998).
11. S. Ryu, S. Zhou, A. G. Ladurner, R. Tjian, *Nature* **397**, 446 (1999).
12. A. M. Näär *et al.*, *Nature* **398**, 828 (1999).
13. S. Ryu and R. Tjian, *Proc. Natl. Acad. Sci. U.S.A.* **96**, 7137 (1999).
14. M. Radermacher *et al.*, *J. Microsc.* **146**, 113 (1987).
15. J. Frank *et al.*, *J. Struct. Biol.* **116**, 190 (1996).
16. J. Frank, *Quart. Rev. Biophys.* **23**, 281 (1990).
17. P. A. Penczek, R. A. Grassucci, J. Frank, *Ultramicroscopy* **53**, 251 (1994).
18. G. Harauz and M. van Heel, *Optik* **73**, 146 (1986).
19. N. Kobayashi, T. G. Boyer, A. J. Berk, *Mol. Cell. Biol.* **15**, 6465 (1995); K. H. Emami, A. Jain, S. T. Smale, *Genes Dev.* **11**, 3007 (1997); P. M. Lieberman, J. Ozer, D. B. Gürsel, *Mol. Cell. Biol.* **17**, 6624 (1997).
20. S. M. Ruppert *et al.*, *Hybridoma* **15**, 55 (1996).

21. K. Yokomori *et al.*, *Genes Dev.* **7**, 2235 (1993).
22. R. D. Klemm *et al.*, *Proc. Natl. Acad. Sci. U.S.A.* **92**, 5788 (1995); R. Hori, S. Pyo, M. Carey, *Proc. Natl. Acad. Sci. U.S.A.* **92**, 6047 (1995).
23. S. Malik, D. K. Lee, R. G. Roeder, *Mol. Cell. Biol.* **13**, 6253 (1993); Y. Li *et al.*, *Science* **263**, 805 (1994).
24. R. O. Weinzierl, B. D. Dynlacht, R. Tjian, *Nature* **362**, 511 (1993); R. O. Weinzierl *et al.*, *EMBO J.* **12**, 5303 (1993); S. K. Hansen and R. Tjian, *Cell* **82**, 565 (1995); J. L. Chen and R. Tjian, *Methods Enzymol.* **273**, 208 (1996).
25. F. Andel III, A. G. Ladurner, C. Inouye, R. Tjian, E. Nogales, data not shown.
26. We thank R. Glaeser, W. Nicholson, and K. Downing for helpful discussions and O. Arum for help in scanning micrographs. Supported by grants from the NIH General Medical Sciences (E.N.) the NIH Cancer Institute (R.T.), and the U.S. Department of Energy in contract with the University of California (E.N.).

14 September 1999; accepted 2 November 1999

Control of Early Viral and Bacterial Distribution and Disease by Natural Antibodies

Adrian F. Ochsenbein,[1]* Thomas Fehr,[1] Claudia Lutz,[2] Mark Suter,[3] Frank Brombacher,[4] Hans Hengartner,[1] Rolf M. Zinkernagel[1]

Natural antibodies are often dismissed from immunological analysis as "background," but they may play an important role in conferring immunity against infections. In antibody-free mice infected with various viruses or with *Listeria monocytogenes*, viral or bacterial titers in peripheral organs, including the kidney and brain, were 10 to 100 times greater than in antibody-competent mice (and enhanced their susceptibility to some infections), and titers in secondary lymphoid organs were 10 to 100 times lower than in antibody-competent mice. Thus, natural antibodies play a crucial role by preventing pathogen dissemination to vital organs and by improving immunogenicity through enhanced antigen-trapping in secondary lymphoid organs.

The humoral immunity of naïve animals consists of B cells secreting "natural" antibodies representing the spontaneous repertoire of circulating immunoglobulins (Ig's) that mainly belong to the IgM class, although IgG and IgA natural antibodies have also been described (*1*). A major source of natural antibodies seems to be the peritoneal $CD5^+$ B-1 cell subset (*2*). Circulating antibodies against toxins, bacteria, and erythrocytes in the sera of naïve animals were described very early in the history of immunology (*3*). Nevertheless, despite their abundance and early detection, their role, particularly in host protection, remains unclear. Natural antibodies may form part of innate immunity (*4*); may facilitate antigen uptake, processing, and presentation by B lymphocytes via complement and Fc-receptors (*4*); may induce or prevent autoimmune diseases (*1*, *5*); may clear lipopolysaccharides (*6*) and protect against *Streptococcus pneumoniae* (*7*); or may be involved in a hypothetical immunoregulatory idiotype–anti-idiotype network (*8*).

In many virological and immunological assays it is a convenient practice to predilute sera to variable extents, from 1:10 up to 1:80, to avoid so called "nonspecific background" signals; the consequence of this practice is that naturally occurring antibodies are not normally detected or are not registered.

It is recognized that during infections with many cytopathic viruses (such as polio, influenza, and rabies viruses), the presence of early neutralizing antibodies is essential for protection against lethal disease, which often correlates with viral replication in neural tissues (*9*). The possible role of natural antibodies in viral infections has largely remained unexplored. We found a key role of natural antibodies during generalized infections with vesicular stomatitis virus (VSV), lymphocytic choriomeningitis virus (LCMV), vaccinia virus (vacc-WR), or *Listeria monocytogenes*.

Sera from naïve mice assessed by enzyme-linked immunosorbent assays (ELISAs) on purified LCMV- or vaccinia virus–coated plates (*10*) revealed LCMV-specific natural IgM, but not IgG, at a titer of 1:16 (Fig. 1A) or vaccinia-specific natural IgM at a titer of 1:64 (Fig. 1B). LCMV-specific natural antibodies did not detectably neutralize the virus in vitro (*11*), and only LCMV-binding natural antibodies could be assessed (Table 1). *Listeria*-specific natural antibodies were assessed by fluorescence-activated cell sorting (FACS) analysis (Fig. 1C) (*12*); specific natural IgM, but not IgG, antibodies were detectable up to a dilution of 1:16. Sera from naïve C57BL/6 mice were tested for antibodies specific for two different VSV serotypes: VSV–New Jersey (VSV-NJ) and VSV-Indiana (VSV-IND) (*10*). Because VSV glycoprotein (VSV-G) exhibits the neutralizing determinant at its tip, ELISAs with intact VSV measure essentially neutralizing antibodies (Fig. 1, D and E). In all cases, only IgM was detected. Natural G-binding (neutralizing) antibodies to intact VSV-IND did not cross-react with intact VSV-NJ, as shown by the fact that pre-

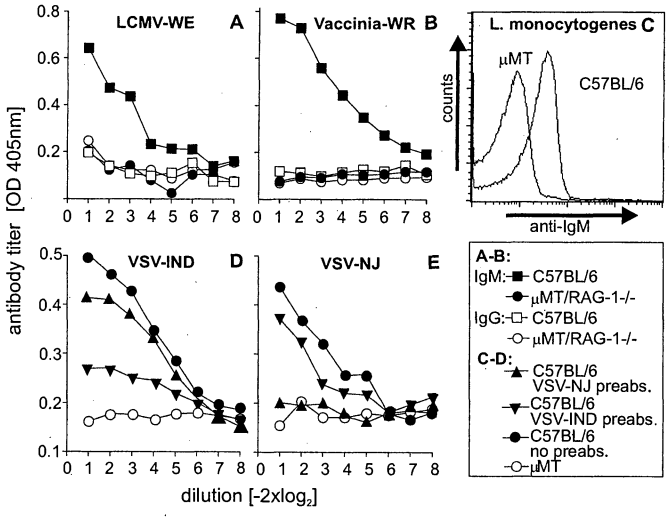

Fig. 1. Detection of natural antibodies. Sera from unimmunized mice were tested in an ELISA (*11*) on purified LCMV-coated (**A**) or purified vacc-WR–coated (**B**) plates for the presence of specific IgM or IgG. (**C**) *Listeria* (5×10^6 CFU) was incubated with 50 μl of prediluted sera (in 1:2 dilution steps; only the 1:4 dilution is shown) from naïve C57BL/6 or μMT mice, stained with fluorescein isothiocyanate–labeled goat anti-mouse IgM^b (from PharMingen) and analyzed by FACS (*12*). Sera of SPF mice were preabsorbed with equal volumes of purified intact VSV-IND or VSV-NJ ($\approx 10^{11}$ PFU/ml) overnight (**D** and **E**) Thereafter, sera were tested either on plates coated with purified VSV-IND (D) or with VSV-NJ (E) virus particles. The mean of three animals per group is shown; variations in the groups were within plus or minus one titer step of 1:2.

[1]Institute for Experimental Immunology, University Hospital Zurich, Schmelzbergstrasse 12, 8091 Zurich, Switzerland. [2]Max Planck Institute for Immunobiology, Freiburg, Germany. [3]M. Suter, Institute for Virology, University of Zurich, Switzerland. [4]F. Brombacher, Department of Immunology, Groote Schuur Hospital, University of Cape Town, 7925 Cape Town, South Africa.

*To whom correspondence should be addressed.

References and Notes

[2] **Functional Domains and Upstream Activation Properties of Cloned Human TATA Binding Protein**
Michael Gregory Peterson; Naoko Tanese; B. Franklin Pugh; Robert Tjian
Science, New Series, Vol. 248, No. 4963. (Jun. 29, 1990), pp. 1625-1630.
Stable URL:
http://links.jstor.org/sici?sici=0036-8075%2819900629%293%3A248%3A4963%3C1625%3AFDAUAP%3E2.0.CO%3B2-4

[8] **Crystal Structure of the Yeast TFIIA/TBP/DNA Complex**
James H. Geiger; Steve Hahn; Sally Lee; Paul B. Sigler
Science, New Series, Vol. 272, No. 5263. (May 10, 1996), pp. 830-836.
Stable URL:
http://links.jstor.org/sici?sici=0036-8075%2819960510%293%3A272%3A5263%3C830%3ACSOTYT%3E2.0.CO%3B2-U

[13] **Purification of Transcription Cofactor Complex CRSP**
Soojin Ryu; Robert Tjian
Proceedings of the National Academy of Sciences of the United States of America, Vol. 96, No. 13. (Jun. 22, 1999), pp. 7137-7142.
Stable URL:
http://links.jstor.org/sici?sici=0027-8424%2819990622%2996%3A13%3C7137%3APOTCCC%3E2.0.CO%3B2-T

LINKED CITATIONS

[22] **Molecular Cloning and Expression of the 32-kDa Subunit of Human TFIID Reveals Interactions with VP16 and TFIIB that Mediate Transcriptional Activation**

Richard D. Klemm; James A. Goodrich; Sharleen Zhou; Robert Tjian

Proceedings of the National Academy of Sciences of the United States of America, Vol. 92, No. 13. (Jun. 20, 1995), pp. 5788-5792.

Stable URL:

http://links.jstor.org/sici?sici=0027-8424%2819950620%2992%3A13%3C5788%3AMCAEOT%3E2.0.CO%3B2-O

[22] **Protease Footprinting Reveals a Surface on Transcription Factor TFIIB that Serves as an Interface for Activators and Coactivators**

Roderick Hori; Sung Pyo; Michael Carey

Proceedings of the National Academy of Sciences of the United States of America, Vol. 92, No. 13. (Jun. 20, 1995), pp. 6047-6051.

Stable URL:

http://links.jstor.org/sici?sici=0027-8424%2819950620%2992%3A13%3C6047%3APFRASO%3E2.0.CO%3B2-Z

[23] **RNA Polymerase II Initiation Factor Interactions and Transcription Start Site Selection**

Yang Li; Peter M. Flanagan; Herbert Tschochner; Roger D. Kornberg

Science, New Series, Vol. 263, No. 5148. (Feb. 11, 1994), pp. 805-807.

Stable URL:

http://links.jstor.org/sici?sici=0036-8075%2819940211%293%3A263%3A5148%3C805%3ARPIIFI%3E2.0.CO%3B2-K